

Experimental Measurement-Device-Independent Certification of Non-Entanglement-Breaking Channels

Yingqiu Mao,^{1,2,*} Yi-Zheng Zhen,^{1,3,*} Hui Liu,^{1,2} Mi Zou,^{1,2} Qi-Jie Tang,^{1,2} Si-Jie Zhang,^{1,2} Jian Wang,^{1,2} Hao Liang,^{1,2} Weijun Zhang,⁴ Hao Li,⁴ Lixing You,⁴ Zhen Wang,⁴ Li Li,^{1,2} Nai-Le Liu,^{1,2} Kai Chen,^{1,2} Teng-Yun Chen,^{1,2} and Jian-Wei Pan^{1,2}

¹*Hefei National Laboratory for Physical Sciences at Microscale and Department of Modern Physics, University of Science and Technology of China, Hefei, Anhui 230026, P. R. China*

²*CAS Center for Excellence and Synergetic Innovation Center in Quantum Information and Quantum Physics, University of Science and Technology of China, Hefei, Anhui 230026, P. R. China*

³*Institute for Quantum Science and Engineering, Southern University of Science and Technology, Shenzhen, Guangdong 518055, P. R. China*

⁴*State Key Laboratory of Functional Materials for Informatics, Shanghai Institute of Microsystem and Information Technology, Chinese Academy of Sciences, Shanghai 200050, P. R. China*

As a crucial ingredient for quantum information tasks, non-entanglement-breaking (non-EB) channels can maintain entanglement for distributing and storing quantum states. Previous methods to test non-EB channels either require an unjustified assumption of fully trusted measurements, or verify correlations inequivalent to entanglement. Here, we demonstrate a measurement-device-independent certification of non-EB channels based on an improved semi-quantum signaling game, which is robust against loss and detection errors. By using realistic sources and considering flawed state preparation, non-EB regions of decoherence channels and noise channels are unveiled. The results show feasibility of certifying non-EB channels without entangled sources, and can be applied to benchmark functions of practical quantum devices.

Entanglement, one of the most intriguing phenomena of quantum theory, has been proven a fundamental resource for state-of-the-art quantum technologies [1–4]. Among them, numerous quantum information tasks have shown better performance than their classical counterparts, when the entanglement between quantum states for the corresponding quantum process is maintained [5–8]. Notably, effective entanglement distribution is a crucial precondition for unconditional security in quantum cryptography [5, 6] while persisting entanglement over computation time is necessary for the speed-up of quantum computing [7].

Such processes require at least the participating channel is non-entanglement-breaking (non-EB), i.e., the channel guarantees non-vanishing entanglement when a party of an entangled pair transmits through it [9]. In contrast, the EB channel corresponds to a measure-and-prepare process, which destroys the coherence of the state and is unable to preserve quantum information [10]. To reveal quantum advantages based on entanglement, it is important to witness that the participating channel is indeed non-EB. This certification is not only fundamentally interesting, but also provides a basic tool in examining the channel's ability to accomplish quantum information tasks.

The intuitive way to certify a non-EB channel is to send one party of an entangled pair through the channel and measure the output bipartite state using a loophole-free Bell test [11–13] or an entanglement witness [1, 2, 14, 15]. Although Bell tests do not assume prior knowledge of experimental devices, they verify a different resource from entanglement, i.e., non-locality [16]. Meanwhile, entanglement witnesses have been proven unrobust to measurements without additional sources [17–20]. An alternative method is to perform quantum process tomography, which enables one to determine the exact process of a quantum channel [21–24]. However, imperfect detection devices may cause reconstruction of nonphysical states [25], which leads to wrong characterizations of the channel. Also, in an adversarial situation, this may even lead to security loopholes [26–29].

Recently, a viable solution to these problems was proposed, where a non-EB channel can be witnessed in the measurement-device-independent (MDI) scenario [30]. By playing a semi-quantum signaling game (SQSG), the non-EB channel is proven as a necessary resource to win (see Fig. 1). In this game, only perfect state preparation is assumed, while the measurement device can be completely uncharacterized. Consequently, effects from detection errors and side-channels can be eliminated, making the certification completely robust to measurement imperfections. Moreover, this MDI approach is loss-insensitive, and is compatible with arbitrarily low detection efficiencies. Furthermore, as no entanglement source and few measurement settings are required, the experimental overheads can be reduced. In this sense, non-EB channels can in principle be certified with minimal assumptions. Still, a faithful and complete demonstration of the MDI certification for non-EB channels is lacking.

In this Letter, we experimentally demonstrate an MDI certification of quantum channels based on an improved SQSG. Considering the non-ideal source with imperfect state preparation, we extend the SQSG to a practical

* These authors contributed equally to this work.

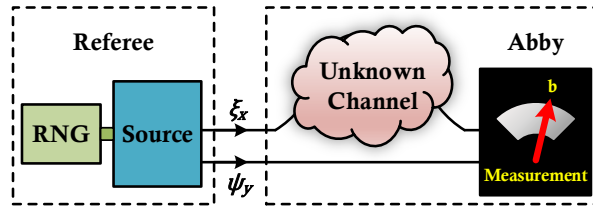


FIG. 1. Schematics of the semi-quantum signaling game [30]. The referee first asks a random quantum question ξ_x to the player Abby, who inputs ξ_x to an unknown channel to be certified. Later, the referee randomly asks another quantum question ψ_y . Then, Abby feeds the channel output and ψ_y into an untrusted measurement device, which yields an answer b . Finally, based on ξ_x , ψ_y , and b , the referee calculates an average payoff, and Abby wins the game if it is larger than 0. RNG: random number generator.

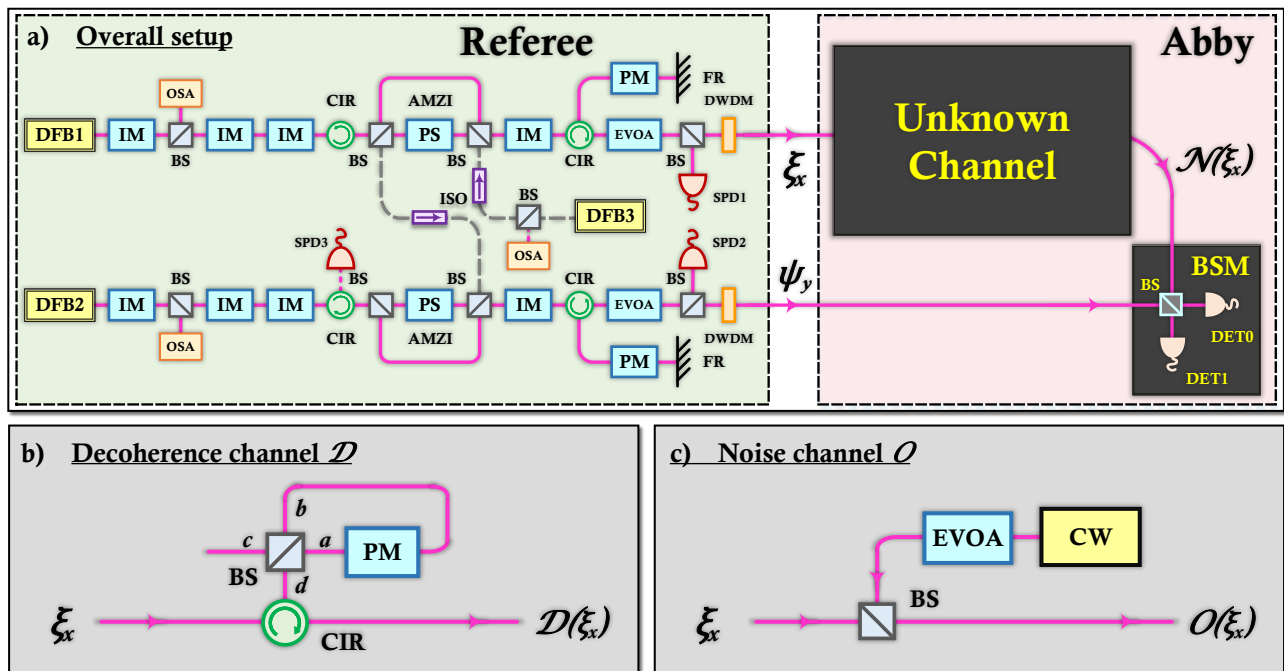


FIG. 2. Experimental setup of MDI certification for non-EB channels. DFB: distributed feedback laser; IM: intensity modulator; AMZI: asymmetric Mach-Zehnder interferometer; BS: beam splitter; CIR: circulator; PS: phase shifter; PM: phase modulator; FR: fiber reflector; EVOA: electronic variable optical attenuator; DWDM: dense wavelength-division multiplexer; SPD: InGaAs gated single photon detector; CW: continuous wave laser source; DET0 and DET1: superconducting nanowire single photon detectors. All fibers used are polarization maintaining fibers.

scenario and give an experimental bound for all EB channels. The certification of the non-EB decoherence channel is observed as a violation of this bound, even when the channel destroys 90% of the state coherence. We further investigate the noise channel and examine the existence of non-EB channel as a precondition for secure key generation in quantum cryptography.

The experimental setup, as shown in Fig. 2a, is composed of two main portions—a referee and a player Abby. The referee randomly asks quantum questions, i.e. sending quantum states, to Abby by randomly preparing states of ξ_x and ψ_y using time-bin and phase encoding [31] with two identical preparation modules. Specifically, for Z basis, $\{|0\rangle_Z, |1\rangle_Z\}$ are encoded in the first and second time-bin, respectively, while for X and Y bases $\{|0\rangle_X, |1\rangle_X, |0\rangle_Y, |1\rangle_Y\}$ are encoded in the relative phase as $\{0, \pi, \pi/2, 3\pi/2\}$ between the two time-bins, respectively.

The optical signals are sent from DFB1 (DFB2) at wavelength of 1550.12 nm with 37.5 MHz repetition rate. By using an IM, the optical pulses are narrowed to 2.5 ns at FWHM. The time-bins are created using an AMZI that separates the pulses at 6.5 ns, and the basis information of Z or X (Y) is chosen with the following IM. For phase encoding, by using the FR, the optical pulses travel through the PM twice for lower modulation voltage. In addition, another IM is used to adjust the intensity difference between pulses of Z and X (Y) bases. All IMs

and PMs for preparing ξ_x and ψ_y are controlled by independent random numbers. The pulses are lowered down to single photon level with an EVOA, and are filtered with a 100 GHz DWDM for spectral noise.

To perform the MDI certification, the referee first generates a pulse of ξ_x . Abby receives ξ_x and input it to the unknown channel \mathcal{N} , which outputs $\mathcal{N}(\xi_x)$. Then, the referee generates a second pulse of ψ_y . Based on an untrusted measurement implemented with the partial Bell-state measurements (BSM), Abby replies with an answer b . The BSM is composed of a BS and two superconducting nanowire single photon detectors (SNSPD). When coincidence counts occur at two alternative time bins of Det0 and Det1, projection on the singlet state $|\Psi^-\rangle = (|01\rangle - |10\rangle)/\sqrt{2}$ is selected, which Abby labels $b = 0$. Otherwise, $b = 1$. To compensate the difference in arrival time to the BSM for pulses $\mathcal{N}(\xi_x)$ and ψ_y , DFB1 and DFB2 alternatively send pulses to the SNSPDs, where an arrival time difference is calculated. By adjusting the pulse delays with a programmable delay chip, $\mathcal{N}(\xi_x)$ and ψ_y pulses are precisely overlapped at the BS. The detection efficiency is 27% and the dark count rate is 50 counts per second for each detector. The effective time window is set to $\sim 85\%$, which is an optimal trade-off between effective coincidence count rates and eliminating imperfect phase encodings at the pulse edges of X and Y basis.

Based on states ξ_x and ψ_y , as well as b , the referee assigns a payoff function $\wp(b, x, y)$ to Abby to indicate how much she will earn or lose. We denote $P_{\mathcal{N}}(b|\xi_x, \psi_y)$ as the probability for Abby to reply b by jointly measuring $\mathcal{N}(\xi_x)$ and ψ_y . The average payoff is written as

$$I_{\mathcal{N}} = \sum_{x,y,b} \wp(b, x, y) P_{\mathcal{N}}(b|\xi_x, \psi_y). \quad (1)$$

For every non-EB channel, there always exists a specific SQSG, such that Abby can obtain a positive average payoff, while $I_{\mathcal{N}_{EB}} \leq 0$ for all EB channels \mathcal{N}_{EB} [30]. The identity channel yields the largest average payoff, which corresponds to 0.5. The specific SQSG for this experiment is expressed and discussed in the Appendix [32].

However, this ideal bound 0 holds only when quantum questions are perfectly prepared. In practice, preparations of ξ_x and ψ_y are in general flawed with realistic devices, and the bound may become a different value. To avoid falsely witnessing non-EB channels, a correction to the ideal bound is necessary. Here, based on the assumption that the referee has full knowledge of states ξ_x and ψ_y , an experimental bound can be derived as

$$C_{EB} = \max_{\mathcal{N}_{EB}} \sum_{x,y,b} \wp(b, x, y) P_{\mathcal{N}_{EB}}(b|\xi_x, \psi_y), \quad (2)$$

where the maximization is taken over all EB channels. Thus, the inequality $I_L > C_{EB}$ guarantees the non-EB property of the tested channel. In our experiment, the ideal bound 0 for all EB channels is increased to 0.047 (more details of the experimental bound are shown in [32]).

Furthermore, the average payoff Eq. (1) holds strictly when pulses of ξ_x and ψ_y are implemented with ideal single photons. As phase-randomized weak coherent pulses (WCPs) are used in the experiment, pulses of ξ_x and ψ_y contain large portions of vacuum and multiphoton emissions. We use the decoy-state method [33–35] to evaluate the probability of single-photon detection events, denoted as Y_{b,ξ_x,ψ_y}^{11} instead of $P_{\mathcal{N}}(b|\xi_x, \psi_y)$. By sending pulses of ξ_x and ψ_y with different intensities, Y_{b,ξ_x,ψ_y}^{11} can be lower and upper bounded as $Y_{b,\xi_x,\psi_y}^{11,L}$ and $Y_{b,\xi_x,\psi_y}^{11,U}$, respectively.

$$I_L = \sum_{b,x,y} \wp(b, x, y) Y_{b,\xi_x,\psi_y}^{1,1,L/U}, \quad (3)$$

where $Y_{\xi_x,\psi_y}^{11,L}$ or $Y_{\xi_x,\psi_y}^{11,U}$ are taken in according to the sign of $\wp(b, x, y)$. In the experiment, the decoy intensities are modulated with an IM to implement the signal, decoy and vacuum states with mean photon number per pulse of 0.03, 0.02, and 0, respectively for both ξ_x and ψ_y . We leave the calculation of I_L in the Supplemental Material [32].

As a demonstration of our approach, we test the decoherence channel, which arguably characterizes the most typical process in the quantum memory. After transmission, the coherence of the state is suppressed and the information of the system is lost [10]. With the all-fiber system, the decoherence channel is implemented with a Sagnac interferometer, as shown in Fig. 2b and discussed in [32]. This process can be described as

$$\mathcal{D}_\gamma(\rho) = (1 - \gamma)\rho + \gamma(|0\rangle\langle 0|_Z \rho_{00} + |1\rangle\langle 1|_Z \rho_{11}), \quad (4)$$

with $\rho_{00} = \langle 0|\rho|0\rangle_Z$ and $\rho_{11} = \langle 1|\rho|1\rangle_Z$. The coherence in $\mathcal{D}_\gamma(\rho)$ is suppressed when γ increases, and \mathcal{D}_γ becomes EB if and only if $\gamma = 1$.

As shown in Fig. 3, the results I_L lower bounds the green line of I , which shows good accordance between experimental results and theoretical predictions. For $\gamma \in \{0, 0.1, 0.3, 0.6\}$, the corresponding I_L are all larger than the experimental bound, indicating their non-EB characteristic. For $0.9 \leq \gamma < 1$, subtle violation of the experimental bound is observed considering statistical fluctuations. Nevertheless, such non-EB channels preserve very weak entanglement (or coherence) and may be of little use in practice. For $\gamma = 1$, I_L does not violate the

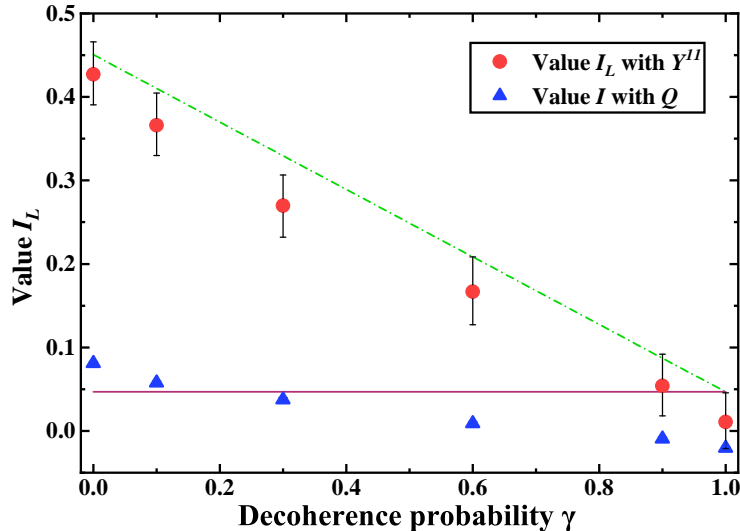


FIG. 3. Performance of the MDI certification for the decoherence channel. The red dots are values of I_L based on the decoy-state method, with black bars referring to statistical fluctuations of 1 standard deviation. The green dash-dot line represents the theoretical I considering detection efficiency and state preparation imperfections, and the solid line represents the experimental bound. The blue triangles are values of I obtained with WCPs directly.

experimental bound, which is in accordance with the theory that the fully decoherence channel is EB. This positive value of I_L shows the practical value of the experimental bound, when compared with the ideal bound 0.

In addition, we compare the MDI certification using WCPs with and without the decoy-state method. As shown in Fig. 3, when only WCPs are used, channels of $\gamma \in \{0, 0.1\}$ can be certified, while those of $\gamma \in \{0.3, 0.6, 0.9, 1\}$ is unknown. This is mainly because multiphoton detection events, which are mostly two-photon emissions, cannot be excluded efficiently with WCPs only. In some cases, these multiphoton pulses may open security loopholes such that an adversary can obtain the encoding information [36], which may even lead to a fake violation. By using the decoy-state method, vacuum and multiphoton detection events can be eliminated, and the conditioned probability of single photon detection events can be obtained. The compatibility of the decoy-state WCPs with MDI certification is thus shown with practicality.

As another application of our approach to investigate realistic channels, we further test another typical quantum channel, where extra noise states are combined with the original input. Such channels, termed noise channel here, frequently appear in practice. For instance, when co-existing quantum key distribution (QKD) with classical communications in a single fiber using wavelength-division multiplexing, the Raman scattering noise photons generated by classical signals are unavoidably mixed with the quantum pulses, thus reducing the secure key rate [37–39]. Here, we implement such a channel by combining extra photons from a CW source with the ξ_x pulses (as shown in Fig 2c). We refer to the ratio of CW intensity to ξ_x pulse intensity per second, denoted by β , as the strength of noise.

As shown in Fig. 4, the noise channel is certified non-EB when β is less than 0.35. When $\beta > 0.35$, under present settings, the non-EB property is unknown. Additionally, when ξ_x is completely replaced by noise photons, i.e., when the information of input states ξ_x is completely lost, the value I_L is -0.43 (not drawn in Fig. 4). To gain a better understanding of the link between our approach and other quantum information tasks, we simulate the secure key rate of MDI-QKD for each β [40], with the calculation shown in the Appendix [32]. Interestingly, the simulation for secure key rate drops to zero before the channel transitions from non-EB to unknown. This suggests that while the channel may still be non-EB, the correlation has been fatally weakened such that a secure key can not be extracted in the current setting. Thus, we observe that the existence of non-EB channel is a precondition for establishing secure keys [6]. Additionally, such results indicate the potential application of our approach to test the feasibility of QKD on specific quantum channels, instead of implementing QKD protocols directly.

In summary, we have demonstrated an experimental MDI certification of non-EB channels in an all fiber system. We have generalized the SQSG to realistic experimental settings, and provided an experimental bound based on full characterization of the source. We further avoid false certification by excluding multiphoton contributions from the WCPs using the decoy-state method. Our approach is then explicitly tested in two typical quantum channels. The violation of experimental bound is observed in the decoherence channel, showing a good accordance with theoretical predictions. Moreover, we have studied the noise channel by exploring the link between the non-EB property and secure key generation of MDI-QKD.

We remark that the decoy-state method can be used for sources other than WCPs. Also, the SQSG with practical

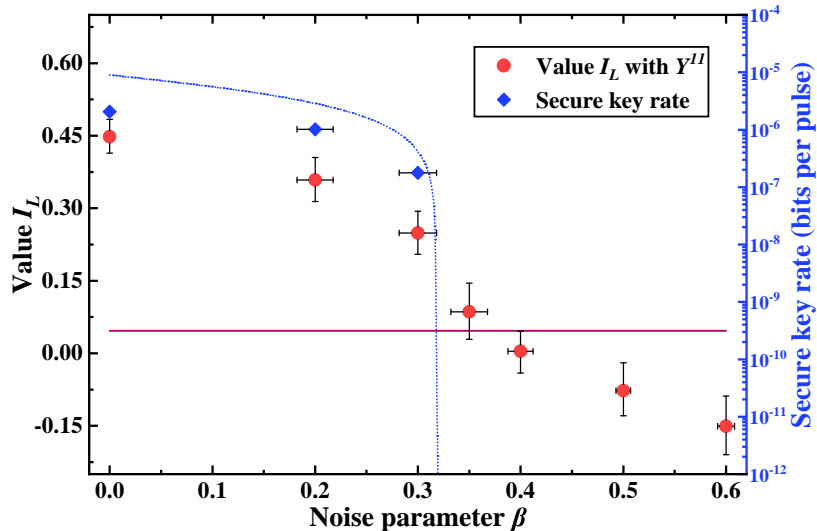


FIG. 4. Performance of the MDI certification for the noise channel. The red dots are values I_L , with black bars referring to the statistical fluctuations of 1 standard deviation. The solid line represents the experimental bound. For the secure key rate R , the blue diamonds are key rates based on the experimental data, while the blue dotted line represents the simulated key rate with our experimental parameters. When $R < 0$, no secure keys are generated.

state preparations, as discussed in this work, can be extended beyond optical fiber systems. Thus, our approach can be further adapted to certify the functions of realistic quantum devices such as quantum memories and quantum gates, and is a step forward in bridging the gap between theory and practice for justifying quantum advantages of novel quantum technologies.

Acknowledgments

We especially thank Francesco Buscemi for enlightening and generous discussions on quantum channels. We also thank Jun Zhang, Wen-Yuan Wang, Yan-Lin Tang, Ping Xu, and Qinghe Mao for valuable discussions.

This work has been supported by the National Key R&D Program of China (2017YFA0303903), the Chinese Academy of Science, the National Fundamental Research Program, the National Natural Science Foundation of China (Grant No. 61875182, No. 11575174, No. 11874346, and No. 11574297), Anhui Initiative in Quantum Information Technologies, and Fundamental Research Funds for the Central Universities (WK2340000083).

Appendix A: The MDI certification of non-EB channels

In this section, we discuss the measurement-device-independent (MDI) certification of non-entanglement-breaking (non-EB) channels based on the semi-quantum signaling game (SQSG), and then extend the theory to the realistic settings by tackling imperfect state preparation and multi-photon emissions from the source.

1. The SQSG

The SQSG offers an operational method to distinguish a non-EB channel from all EB ones, as proven in Rosset, Buscemi, and Liang's seminal paper [30]. In this game (see Fig. 1 in the main text), the referee first randomly asks a quantum question, i.e., sending a quantum state ξ_x , to the player Abby, who has the unknown channel \mathcal{N} to be tested. Abby inputs ξ_x to \mathcal{N} and obtain an output state $\mathcal{N}(\xi_x)$. Then, the referee randomly asks another quantum question ψ_y . Using an untrusted measurement device, Abby replies with an answer b .

The payoff function, denoted by $\varphi(b, x, y)$, describes how much Abby will earn or lose with answer b given questions ξ_x and ψ_y . After the game, the average payoff is announced by the referee and written as

$$I_{\mathcal{N}} = \sum_{x,y,b} \varphi(b, x, y) P_{\mathcal{N}}(b|\xi_x, \psi_y), \quad (\text{A1})$$

where $P_{\mathcal{N}}(b|\xi_x, \psi_y)$ is the probability of obtaining b by measuring $\mathcal{N}(\xi_x)$ and ψ_y . As no further assumptions are made on the measurements, the SQSG is performed in the MDI scenario.

Theoretically, the channel \mathcal{N} is non-EB if and only if the corresponding Choi state, defined as $\sigma_{\mathcal{N}} = \text{id} \otimes \mathcal{N}(\Phi^+)$, is entangled [41], where Φ^+ is the maximally entangled state. In the SQSG, for a specific non-EB channel \mathcal{N} , quantum questions ξ_x and ψ_y , and payoff function $\wp(b, x, y)$ can be selected to construct an entanglement witness (EW) $-W$ for $\sigma_{\mathcal{N}}$ as

$$W = \sum_{x,y} \wp(x, y) \xi_x^T \otimes \psi_y^T, \quad (\text{A2})$$

where $\wp(b=0, x, y) = \wp(x, y)$ and $\wp(b=1, x, y) = 0$ has been assumed. The payoff value $I_{\mathcal{N}}$ is then always less than 0 for EB channels \mathcal{N}_{EB} [30].

In this experiment, we prepare quantum questions as the eigenstates of the Pauli matrices, i.e., $\xi_x, \psi_y \in \{|0\rangle_Z, |1\rangle_Z, |0\rangle_X, |1\rangle_X, |0\rangle_Y, |1\rangle_Y\}$. The payoff function is defined accordingly as

$$\wp(\xi_x, \psi_y) = \begin{cases} \frac{1}{4}, & (\xi_x, \psi_y) \text{ anti-correlated in } X \text{ or } Z; \\ -\frac{1}{4}, & (\xi_x, \psi_y) \text{ correlated in } X \text{ or } Z; \\ -\frac{1}{2}, & (\xi_x, \psi_y) \text{ correlated in } Y; \\ 0, & \text{otherwise.} \end{cases} \quad (\text{A3})$$

Here, ‘‘anti-correlated’’ means (0,1) or (1,0) in the respective bases and ‘‘correlated’’ means (0,0) or (1,1) in the respective bases. Thus, an entanglement witness in the form of

$$-W = \frac{\mathbb{1}}{2} - \Psi^-, \quad (\text{A4})$$

is constructed, with Ψ^- as the projector onto the singlet state, i.e., $|\Psi^-\rangle = (|0\rangle_Z |1\rangle_Z - |1\rangle_Z |0\rangle_Z) / \sqrt{2}$. When the input states ξ_x and ψ_y are prepared *perfectly*, the inequality $I_{\mathcal{N}} > 0$ certifies a non-EB channel \mathcal{N} .

2. The experimental bound

The EB channel \mathcal{N}_{EB} is in general a measure-and-prepare channel, i.e.,

$$\mathcal{N}_{EB}(\rho) = \sum_k \text{tr}[E_k \rho] \gamma_k,$$

where $\{E_k | E_k \geq 0, \sum_k E_k = \mathbb{1}\}$ is a set of POVMs and $\{\gamma_k\}$ is a set of quantum states. In the SQSG, the average payoff of \mathcal{N}_{EB} can then be bounded by

$$\begin{aligned} C_{EB} &= \max_{\mathcal{N}_{EB}} I_{\mathcal{N}_{EB}} = \max_{\mathcal{N}_{EB}} \sum_{x,y} \wp(x, y) P_{\mathcal{N}_{EB}}(0|\xi_x, \psi_y) \\ &= \max_{\mathcal{N}_{EB}, M} \sum_{x,y} \wp(x, y) \text{tr}[\mathcal{N}_{EB}(\xi_x) \otimes \psi_y M] \\ &= \max_{E_k, F_k} \sum_{x,y,k} \wp(x, y) \text{tr}[E_k \xi_x] \text{tr}[\gamma_k \otimes \psi_y M] \\ &= \max_{E_k, F_k} \text{tr} \left[W \sum_k E_k^T \otimes F(k)^T \right], \end{aligned} \quad (\text{A5})$$

where M and $F(k) = \text{tr}_1[\gamma_k \otimes \mathbb{1}M]$ are POVMs acting on $\mathcal{N}_{EB}(\xi_x) \otimes \psi_y$ and ψ_y , respectively. When $-W$ is an EW and ξ_x and ψ_y are prepared perfectly, bound C_{EB} is 0 as $E_k^T \otimes F(k)^T$ are separable positive operators, i.e., $\text{tr}[W E_k^T \otimes F(k)^T] \leq 0$ holds for all k . However, in realistic experiments, the quantum states are unavoidably prepared with errors. In this case, denote the states prepared as $\tilde{\xi}_x$ and $\tilde{\psi}_y$, respectively. Also, $\sum_k E_k^T \otimes F(k)^T$ can be bounded as

$$\begin{aligned} \sum_k E_k^T \otimes F(k)^T &= d^2 \sum_k \frac{\text{tr}[E_k^T] \text{tr}[F(k)^T]}{d^2} \frac{E_k^T}{\text{tr}[E_k^T]} \otimes \frac{F(k)^T}{\text{tr}[F(k)^T]} \\ &\leq d^2 \omega_{sep} \end{aligned} \quad (\text{A6})$$

where ω_{sep} is a separable states. To see this, notice that

$$\sum_k \text{tr}[E_k] \text{tr}[F(k)] = \text{tr}[\mathcal{N}_{EB}(\mathbb{1}) \otimes \mathbb{1}M] \leq d^2 \text{tr}[\mathcal{N}_{EB}(\rho_{mix}) \otimes \rho_{mix}M] \leq d^2, \quad (\text{A7})$$

where $\rho_{mix} = \mathbb{1}/d$ is the maximally mixed state. Thus, the experimental bound can be calculated as

$$\begin{aligned} C_{EB}^{exp} &= \max_{E_k, F_k} \text{tr} \left[\tilde{W} \sum_k E_k^T \otimes F(k)^T \right] \\ &= d^2 \max_{\omega_{sep}} \text{tr} \left[\tilde{W} \omega_{sep} \right]. \end{aligned} \quad (\text{A8})$$

Based on the assumption that the referee has full knowledge of the quantum questions, in the experiment, the referee can use the state tomography to determine the density matrices of the prepared states (as shown in Sec. B4). The experimental EB bound is numerically calculated as 0.0468, higher than the ideal bound of 0. Additionally, by replacing the maximization in Eq. (A8) with that over all 2-qubit states, the maximal value of $I_{\mathcal{N}}$ can be also calculated, which is a value of 0.4506, a little lower than 0.5 of the ideal case.

3. Evaluation of single-photon detections

In this experiment, we apply the decoy-state method to the weak coherent pulses (WCP), which can efficiently evaluate the single-photon detection events [33, 34, 42]. Generally, the quantum states of phase-randomized WCPs can be written in the Fock basis as

$$\rho_\alpha = e^{-\alpha} \sum_{n=0}^{\infty} \frac{\alpha^n}{n!} |n\rangle \langle n|, \quad (\text{A9})$$

where α is the mean photon number per pulse and n is the photon number. When pulses ξ_x and ψ_y are prepared with intensities α_ξ and α_ψ , respectively, the probability to obtain the result b of a jointly measurement can be written as

$$Q_{b, \xi_x, \psi_y}^{\alpha_\xi \alpha_\psi} = e^{-\alpha_\xi - \alpha_\psi} \sum_{n, m=0}^{\infty} \frac{\alpha_\xi^n \alpha_\psi^m}{n! m!} Y_{b, \xi_x, \psi_y}^{nm}. \quad (\text{A10})$$

In the experiment, $Q_{\xi_x, \psi_y}^{b, \alpha_\xi \alpha_\psi}$ is the ratio of the number of detection events to the number of emitted pulse pairs in ξ_x and ψ_y with mean photon numbers α_ξ and α_ψ , respectively. Consequently, $Y_{b, \xi_x, \psi_y}^{nm}$ is the conditional probability of detection events b given that n -photon and m -photon pulses are emitted in ξ_x and ψ_y , respectively [40, 43].

The decoy-state method is applied when ξ_x and ψ_y are randomly prepared with different intensities. In this experiment, three types of mean photon per pulse values, i.e., $\alpha_\xi, \alpha_\psi \in \{\mu, \nu, \omega | \mu > \nu > \omega = 0\}$, are used. Thus, seven gains of $Q_{\xi_x, \psi_y}^{\alpha_\xi \alpha_\psi}$ with $\{\alpha_\xi \alpha_\psi\} \in \{\mu\mu, \nu\nu, \mu\omega, \omega\mu, \nu\omega, \omega\nu, \omega\omega\}$ can be obtained. We first consider J_1 and J_2 in the form of (ξ_x and ψ_y are omitted for simplicity),

$$\begin{aligned} J_1 &= Q_{\nu\nu} e^{2\nu} + Q_{\omega\omega} - Q_{\nu\omega} e^\nu - Q_{\omega\nu} e^\nu, \\ J_2 &= Q_{\mu\mu} e^{2\mu} + Q_{\omega\omega} - Q_{\mu\omega} e^\mu - Q_{\omega\mu} e^\mu, \end{aligned} \quad (\text{A11})$$

and then calculate the equation $\mu^3 J_1 - \nu^3 J_2$, where $Y^{n,0}, Y^{0,m}$ and $Y^{1,2}, Y^{2,1}$ can be canceled. We obtain

$$\begin{aligned} Y^{11} &= \frac{\mu^3 J_1 - \nu^3 J_2}{\mu^2 \nu^2 (\mu - \nu)} \\ &\quad - \frac{1}{\mu^2 \nu^2 (\mu - \nu)} \sum_{n, m \geq 2} \frac{\mu^3 \nu^{n+m} - \nu^3 \mu^{n+m}}{n! m!} Y^{nm}. \end{aligned} \quad (\text{A12})$$

Since $Y^{n,m} \in [0, 1]$ and $\mu > \nu$, the lower bound $Y^{1,1,L}$ and upper bound $Y^{1,1,U}$ can be written as

$$\begin{aligned} Y^{11,L} &= \frac{\mu^3 J_1 - \nu^3 J_2}{\mu^2 \nu^2 (\mu - \nu)}, \\ Y^{11,U} &= Y^{11,L} - \frac{\mu^3 (e^\nu - 1 - \nu)^2 - \nu^3 (e^\mu - 1 - \mu)^2}{\mu^2 \nu^2 (\mu - \nu)}, \end{aligned} \quad (\text{A13})$$

respectively. Finally, by replacing $P_{\mathcal{N}}(b|\xi_x, \psi_y)$ with $Y^{1,1,L}$ or $Y^{1,1,U}$ accordingly, the lower bound of the payoff value $I_{\mathcal{N}}$ can be written as

$$\begin{aligned}
I_L = & -\frac{1}{4}Y_{0z0z}^{11,U} + \frac{1}{4}Y_{0z1z}^{11,L} + \frac{1}{4}Y_{1z0z}^{11,L} - \frac{1}{4}Y_{1z1z}^{11,U} \\
& -\frac{1}{4}Y_{0x0x}^{11,U} + \frac{1}{4}Y_{0x1x}^{11,L} + \frac{1}{4}Y_{1x0x}^{11,L} - \frac{1}{4}Y_{1x1x}^{11,U} \\
& -\frac{1}{2}Y_{0y0y}^{11,U} - \frac{1}{2}Y_{1y1y}^{11,U}.
\end{aligned} \tag{A14}$$

Therefore, the observation of $I_L > C_{EB}^{exp}$ indicates that Abby wins the SQSG, and implies that the tested channel \mathcal{N} is non-EB.

Appendix B: Experiment details

In this section, we introduce the basic techniques of the experiments, including feedback systems and the design and implementation of the decoherence channel and noise channel. Also, the robustness of this approach against variations of prepared states is explicitly studied according to quantum state tomography.

1. Feedback systems

We adopt feedback systems for phase, optical intensity, wavelength, and bias voltage to ensure the stability of the entire system.

In order to obtain high interference visibility in the X and Y basis at the Bell-state measurement (BSM), a phase reference needs to be established between the two state preparation modules, i.e., the phase difference between the two asymmetric Mach-Zehnder interferometers (AMZI) should be $2\pi k$, with k a positive integer. Pulses of wavelength 1550.12 nm and frequency of 25 MHz are sent from DFB3 through the two AMZI in sequence, as shown in Fig. 2 in the main text. Here, the pulses can be detected in three time-windows, where only that in the second time window show interference. A gated InGaAs single-photon detector (SPD) is used to detect the interference photons, and the 2π phase drift of the AMZIs is measured to be ~ 8 minutes. For the experiment, a real-time phase feedback system is built. A fiber phase shifter is placed on the short arm of AMZI1 to maintain the interference steady at destructive interference, i.e., the interference photons are monitored with the SPD to remain minimum photon count. Thus, the phase reference between ξ_x and ψ_y is established.

For optimal BSM, firstly the arrival time of both ξ_x and ψ_y pulses are calibrated at the BSM site. Here, signals are alternatively sent from DFB1 and DFB2 to the superconducting nanowire SPDs, where an arrival time difference is calculated. By adjusting the pulse delays with a programmable delay chip, ξ_x and ψ_y pulses are precisely overlapped. Secondly, the wavelengths of both ξ_x and ψ_y are required to be almost the same. Here, the temperature of DFB2 is scanned, and the Hong-Ou-Mandel dip is measured. The temperature set to the value where minimum coincidence count occurs, which is 55%. Thus the wavelengths are optimal. Thirdly, considering the fluctuations of the source and bias voltages of IMs, the intensities of ξ_x and ψ_y pulses are calibrated every ~ 600 seconds.

In addition, the clock reference for the entire system is established by sending synchronization laser pulses at 1570 nm of 500 kHz through a separate fiber to each of ξ_x and ψ_y state preparation modules. Then, they are detected through a photodiode and the system repetition rate of 37.5 MHz is generated. With this configuration, we optimized pulse modulation from the modulators such that fast real-time data acquisition is realized.

2. Realization of the decoherence channel through the Sagnac interferometer

As discussed in the maintext, the decoherence channel preserves populations of the state in the Z basis, while the coherence between them, i.e., information of the relative phases, is suppressed. To realize such a channel, we design the Sagnac interferometer (SI) with a phase modulator (PM) to randomly eliminate the first or second time-bin when states in X and Y bases are prepared. Initially, four input states $|0\rangle_X, |1\rangle_X, |0\rangle_Y, |1\rangle_Y$ are encoded in the phase between first and second time-bins, written as $|\sqrt{\alpha/2}\rangle^s |e^{i\phi}\sqrt{\alpha/2}\rangle^l$ with $\phi = 0, \pi, \pi/2, 3\pi/2$ for simplicity. Here, s and l represent the short and long arm of the AMZI, respectively.

As shown in Fig. 2b of the main text, when entering the SI, ξ_x is firstly split into two paths a and b by the beam splitter (BS), with path a a shorter arrival time to the PM than that of path b . Then, ξ_x is split into four pulses. By exactly adjusting the length of paths a and b , we set the arrival time for the pulses of two paths in a difference

of 13.3 ns. Now, the time-bins in the sequence of $|\sqrt{\alpha}/2\rangle_a^s, |e^{i\phi}\sqrt{\alpha}/2\rangle_a^l, |\sqrt{\alpha}/2\rangle_b^s, |e^{i\phi}\sqrt{\alpha}/2\rangle_b^l$ are modulated by the PM, adding relative phases $\theta_a^s, \theta_a^l, \theta_b^s, \theta_b^l$. Below we write the exact process for ξ_x to transmit through the SI,

$$\begin{aligned} & \left| \sqrt{\frac{\alpha}{2}} \right\rangle \left| e^{i\phi} \sqrt{\frac{\alpha}{2}} \right\rangle \xrightarrow{BS} \left| i \frac{\sqrt{\alpha}}{2} \right\rangle_a^s \left| i e^{i\phi} \frac{\sqrt{\alpha}}{2} \right\rangle_a^l \left| \frac{\sqrt{\alpha}}{2} \right\rangle_b^s \left| e^{i\phi} \frac{\sqrt{\alpha}}{2} \right\rangle_b^l \xrightarrow{PM} \left| i e^{i\theta_a^r} \frac{\sqrt{\alpha}}{2} \right\rangle_a^s \left| i e^{i(\phi+\theta_a^s)} \frac{\sqrt{\alpha}}{2} \right\rangle_a^l \left| e^{i\theta_b^r} \frac{\sqrt{\alpha}}{2} \right\rangle_b^s \left| e^{i(\phi+\theta_b^s)} \frac{\sqrt{\alpha}}{2} \right\rangle_b^l \\ & \xrightarrow{BS} \left| \left(e^{i\theta_b^r} - e^{i\theta_a^r} \right) \frac{\sqrt{\alpha}}{2\sqrt{2}} \right\rangle_c^s \left| e^{i\phi} \left(e^{i\theta_b^s} - e^{i\theta_a^s} \right) \frac{\sqrt{\alpha}}{2\sqrt{2}} \right\rangle_c^l \left| \left(e^{i\theta_a^r} + e^{i\theta_b^r} \right) \frac{\sqrt{\alpha}}{2\sqrt{2}} \right\rangle_d^s \left| e^{i\phi} \left(e^{i\theta_a^s} + e^{i\theta_b^s} \right) \frac{\sqrt{\alpha}}{2\sqrt{2}} \right\rangle_d^l. \end{aligned}$$

In the experiment, port d is used for the output to the BSM. By adjusting the modulation voltages on the PM for $\theta_a^s, \theta_a^l, \theta_b^s, \theta_b^l$, the channel can either model the identity channel or the fully decoherence channel. Precisely, the identity channel is realized when the PM is turned off, i.e., adding phases 0, 0, 0, 0 in the same sequence. In this case, the state remains the same and is output in port d . As for the fully decoherence channel, we randomly add phases in the sequence 0, 0, 0, π or 0, 0, π , 0 with the same probability, such that the second or first time-bin is eliminated, respectively. The output of port d is thus in the form of $|\sqrt{\alpha}/2\rangle^s$ or $|\sqrt{\alpha}/2\rangle^l$ (up to an overall phase), respectively. By using an independent random number string to control the PM, the identity channel and fully decoherence channel can be realized with probabilities $1 - \gamma$ and γ , respectively. In this manner, decoherence channel of the form

$$\mathcal{D}_\gamma(\rho) = (1 - \gamma)\rho + \gamma(|0\rangle\langle 0|_Z \rho_{00} + |1\rangle\langle 1|_Z \rho_{11}), \quad (\text{B1})$$

can be constructed.

3. The noise channel

We design and realize the noise channel by combining photons of a continuous-wave (CW) source with the WCPs of ξ_x into the untrusted measurement, as shown in Fig. 2c of the main text. The corresponding quantum channel can be regarded as adding extra noise photons into each pulse of ξ_x . We adjust the intensity of the CW, such that different strengths of noise can be modeled. Instead of theoretically analyzing the number of noise photons per pulses, we study this channel from the experimental perspective. To describe the strength of noise, we use the ratio of CW intensity to ξ_x pulse intensity per second, denoted by β .

To calculate the secure key rate, we suppose ξ_x and ψ_y are prepared by two distinct users, namely Alice and Bob, and the BSM is performed by an untrusted third party Charlie in the usual measurement-device-independent quantum key distribution scenario. For both Alice and Bob, pulses of Z basis with intensity μ are used for key generation, and pulses of X basis are used for error estimation. The key rate for measurement-device-independent quantum key distribution is calculated by [40],

$$R \geq Q_{Z,\mu\mu}^{11} (1 - H(e_X^{11})) - Q_Z^{\mu\mu} f H(E_Z^{\mu\mu}). \quad (\text{B2})$$

Here, f is the error correction inefficiency factor, and $H(x) = -x \log_2 x - (1 - x) \log_2 (1 - x)$ is the binary entropy function. $Q_{Z,\mu\mu}^{11}$, $Q_Z^{\mu\mu}$, $E_Z^{\mu\mu}$, and e_X^{11} are the single photon gain, the total gain, the quantum bit error rate in the Z basis, and the quantum bit error rate in the X basis when ξ_x and ψ_y are both of single photons, respectively [40]. The experimental key rates in Fig. 4 of the main text are obtained by taking the measured $Q_Z^{\mu\mu}$ and $E_Z^{\mu\mu}$ into Eq. (B2). The theoretical key rate (dotted) line is obtained by simulating Eq. (B2) with our experimental parameters, where noise photons from the CW are treated as dark counts [39]. Since here our aim is to show the link between non-EB channels and quantum cryptography, the key rate results are not optimized. For higher key rates, one can optimize the mean photon numbers and emission probabilities of the signal and decoy pulses [44], as well as the number of decoys implemented [45].

4. Robustness against flawed state preparation

As discussed in Sec. A2, to avoid falsely witnessing non-EB channels, the experimental bound is determined by the full knowledge of quantum questions. We achieve this by performing state tomography of $\hat{\xi}_x$ and $\hat{\psi}_y$ on the referee's side.

Specifically, we measured the density matrix of an arbitrary qubit state in the form of

$$\rho = \frac{\mathbb{1} + \langle X \rangle X + \langle Y \rangle Y + \langle Z \rangle Z}{2}, \quad (\text{B3})$$

where X , Y , Z are the three Pauli matrices, and $\langle X \rangle$, $\langle Y \rangle$, $\langle Z \rangle$ are expectation values when measuring the corresponding Pauli matrices. In this experiment, $\langle Z \rangle$ of input states is evaluated by a time-bin intensity ratio r , i.e., the ratio of the photon counts in the first time-bin window to that in the second. To obtain $\langle X \rangle$ for each $\tilde{\xi}_x$ (equivalently, $\tilde{\psi}_y$), the pulses of $\tilde{\xi}_x$ ($\tilde{\psi}_y$) are sent through $\tilde{\psi}_y$'s ($\tilde{\xi}_x$'s) AMZI. Photon pulses can be detected at both output ports of the final BS, where they are observed in three consecutive time windows using a gated SPD. Interference is shown in the second time window, where the phase differs π for two ports. By using the photon counts of three time window in both BS outputs, values of $\langle X \rangle$ can be obtained. For the value of $\langle Y \rangle$, we adjust the phase shifter of AMZI1 (see Fig. 2a of the main text), such that two output ports of the final BS correspond to the projection onto relative phases $\pi/2$ and $3\pi/2$ [46].

The constructed density matrices of $\tilde{\xi}_x$ and $\tilde{\psi}_y$ are taking into Eq. (A8), where the experimental bound for all EB channels are derived. Here, we show the tomography results in Fig. 5 and list fidelity [10] of our input states in Table I.

TABLE I. Fidelity of input quantum states

Fidelity(%)	$ 0\rangle$	$ 1\rangle$	$ +\rangle$	$ -\rangle$	$ R\rangle$	$ L\rangle$
$\tilde{\xi}_x$	99.7	99.2	98.4	96.9	97.7	93.6
$\tilde{\psi}_y$	99.5	99.1	99.3	95.7	98.6	94.3

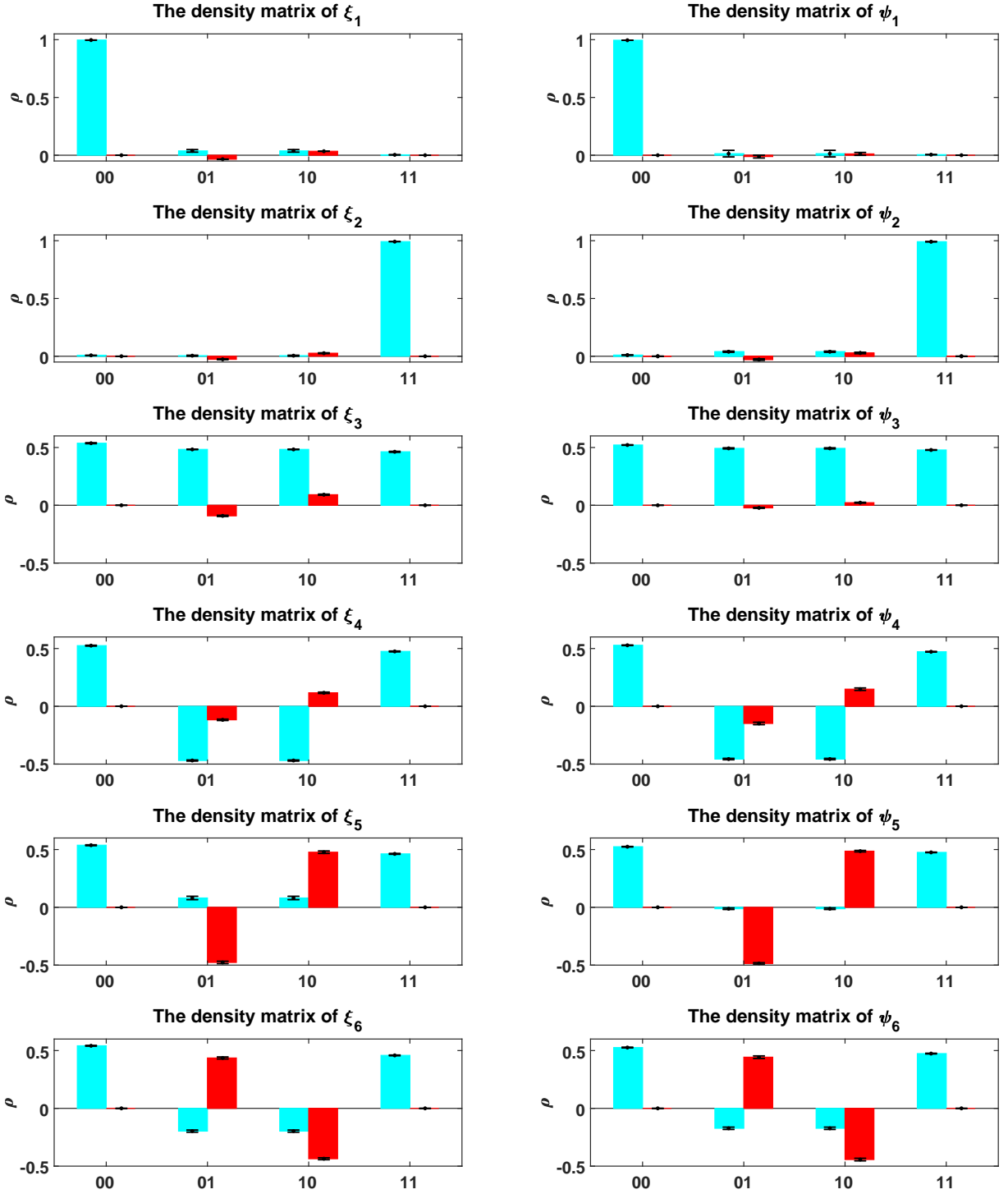


FIG. 5. The tomography results of quantum states used in this experiment. In each figure, four blue bars represent the real part of four entries in the density matrix, while the red bars represent the imaginary part. Based on this description of the quantum states, the referee can determine the bound C_{EB} of all EB channels in the SQSG.

-
- [1] R. Horodecki, P. Horodecki, M. Horodecki, and K. Horodecki, *Rev. Mod. Phys.* **81**, 865 (2009).
[2] O. Gühne and G. Tóth, *Phys. Rep.* **474**, 1 (2009).
[3] N. Brunner, D. Cavalcanti, S. Pironio, V. Scarani, and S. Wehner, *Rev. Mod. Phys.* **86**, 419 (2014).
[4] N. Friis, G. Vitagliano, M. Malik, and M. Huber, *Nat. Rev. Phys.* **1**, 72 (2019).

- [5] M. Curty, M. Lewenstein, and N. Lütkenhaus, Phys. Rev. Lett. **92**, 217903 (2004).
- [6] V. Scarani, H. Bechmann-Pasquinucci, N. J. Cerf, M. Dušek, N. Lütkenhaus, and M. Peev, Rev. Mod. Phys. **81**, 1301 (2009).
- [7] R. Jozsa and N. Linden, Proc. Royal Soc. A **459**, 2011 (2003).
- [8] V. Giovannetti, S. Lloyd, and L. Maccone, Science **306**, 1330 (2004).
- [9] M. Horodecki, P. W. Shor, and M. B. Ruskai, Rev. Math. Phys. **15**, 629 (2003).
- [10] M. A. Nielsen and I. Chuang, “Quantum computation and quantum information,” (2002).
- [11] B. Hensen, H. Bernien, A. E. Dréau, A. Reiserer, N. Kalb, M. S. Blok, J. Ruitenbergh, R. F. Vermeulen, R. N. Schouten, C. Abellán, *et al.*, Nature **526**, 682 (2015).
- [12] M. Giustina, M. A. Versteegh, S. Wengerowsky, J. Handsteiner, A. Hochrainer, K. Phelan, F. Steinlechner, J. Kofler, J.-Å. Larsson, C. Abellán, *et al.*, Phys. Rev. Lett. **115**, 250401 (2015).
- [13] L. K. Shalm, E. Meyer-Scott, B. G. Christensen, P. Bierhorst, M. A. Wayne, M. J. Stevens, T. Gerrits, S. Glancy, D. R. Hamel, M. S. Allman, *et al.*, Phys. Rev. Lett. **115**, 250402 (2015).
- [14] F. Buscemi, Commun. Math. Phys. **310**, 625 (2012).
- [15] F. Buscemi, Phys. Rev. Lett. **108**, 200401 (2012).
- [16] N. Brunner, N. Gisin, and V. Scarani, New Journal of Physics **7**, 88 (2005).
- [17] C. Branciard, D. Rosset, Y. Liang, and N. Gisin, Phys. Rev. Lett. **110**, 060405 (2013).
- [18] P. Xu, X. Yuan, L.-K. Chen, H. Lu, X.-C. Yao, X. Ma, Y.-A. Chen, and J.-W. Pan, Phys. Rev. Lett. **112**, 140506 (2014).
- [19] M. Nawareg, S. Muhammad, E. Amselem, and M. Bourennane, Sci. Rep. **5**, 8048 (2015).
- [20] E. Verbanis, A. Martin, D. Rosset, C. W. Lim, R. Thew, and H. Zbinden, Phys. Rev. Lett. **116**, 190501 (2016).
- [21] J. F. Poyatos, J. I. Cirac, and P. Zoller, Phys. Rev. Lett. **78**, 390 (1997).
- [22] G. M. D’Ariano and P. Lo Presti, Phys. Rev. Lett. **86**, 4195 (2001).
- [23] J. B. Altepeter, D. Branning, E. Jeffrey, T. C. Wei, P. G. Kwiat, R. T. Thew, J. L. O’Brien, M. A. Nielsen, and A. G. White, Phys. Rev. Lett. **90**, 193601 (2003).
- [24] J. L. O’Brien, G. Pryde, A. Gilchrist, D. James, N. K. Langford, T. Ralph, and A. White, Phys. Rev. Lett. **93**, 080502 (2004).
- [25] C. Schwemmer, L. Knips, D. Richart, H. Weinfurter, T. Moroder, M. Kleinmann, and O. Gühne, Phys. Rev. Lett. **114**, 080403 (2015).
- [26] Y. Zhao, C.-H. F. Fung, B. Qi, C. Chen, and H.-K. Lo, Phys. Rev. A **78**, 042333 (2008).
- [27] L. Lydersen, C. Wiechers, C. Wittmann, D. Elser, J. Skaar, and V. Makarov, Nat. photonics **4**, 686 (2010).
- [28] I. Gerhardt, Q. Liu, A. Lamas-Linares, J. Skaar, C. Kurtsiefer, and V. Makarov, Nature Communications **2**, 349 (2011).
- [29] H. Weier, H. Krauss, M. Rau, M. F. Ernst, S. Nauert, and H. Weinfurter, New Journal of Physics **13**, 073024 (2011).
- [30] D. Rosset, F. Buscemi, and Y.-C. Liang, Phys. Rev. X **8**, 021033 (2018).
- [31] X. Ma and M. Razavi, Phys. Rev. A **86**, 062319 (2012).
- [32] See Appendix for details.
- [33] X.-B. Wang, Phys. Rev. Lett. **94**, 230503 (2005).
- [34] H.-K. Lo, X. Ma, and K. Chen, Phys. Rev. Lett. **94**, 230504 (2005).
- [35] X. Ma, C.-H. F. Fung, and M. Razavi, Phys. Rev. A **86**, 052305 (2012).
- [36] G. Brassard, N. Lütkenhaus, T. Mor, and B. C. Sanders, Phys. Rev. Lett. **85**, 1330 (2000).
- [37] P. D. Townsend, Electron. Lett. **33**, 188 (1997).
- [38] B. Fröhlich, M. Lucamarini, J. F. Dynes, L. C. Comandar, W. W.-S. Tam, A. Plews, A. W. Sharpe, Z. Yuan, and A. J. Shields, Optica **4**, 163 (2017).
- [39] Y. Mao, B.-X. Wang, C. Zhao, G. Wang, R. Wang, H. Wang, F. Zhou, J. Nie, Q. Chen, Y. Zhao, Q. Zhang, J. Zhang, T.-Y. Chen, and J.-W. Pan, Opt. Express **26**, 6010 (2018).
- [40] H.-K. Lo, M. Curty, and B. Qi, Phys. Rev. Lett. **108**, 130503 (2012).
- [41] M. Jiang, S. Luo, and S. Fu, Phys. Rev. A **87**, 022310 (2013).
- [42] W.-Y. Hwang, Phys. Rev. Lett. **91**, 057901 (2003).
- [43] F. Xu, M. Curty, B. Qi, and H.-K. Lo, New J. Phys. **15**, 113007 (2013).
- [44] Z.-W. Yu, Y.-H. Zhou, and X.-B. Wang, Phys. Rev. A **91**, 032318 (2015).
- [45] Y.-H. Zhou, Z.-W. Yu, and X.-B. Wang, Phys. Rev. A **93**, 042324 (2016).
- [46] Q.-C. Sun, Y.-L. Mao, S.-J. Chen, W. Zhang, Y.-F. Jiang, Y.-B. Zhang, W.-J. Zhang, S. Miki, T. Yamashita, H. Terai, X. Jiang, T.-Y. Chen, L.-X. You, X.-F. Chen, Z. Wang, J.-Y. Fan, Q. Zhang, and J.-W. Pan, Nat. Photonics **10**, 671 (2016).